ACS APPLIED MATERIALS & INTERFACES

www.acsami.org

Research Article

Intrinsic Isotropic Near-Zero Thermal Expansion in $Zn_4B_6O_{12}X$ (X = O, S, Se)

Youquan Liu,[¶] Dajiang Mei,[¶] Naizheng Wang, Maxim S. Molokeev, Xingxing Jiang,* and Zheshuai Lin*

Cite This: *ACS Appl. Mater. Interfaces* 2020, 12, 38435−38440

Read Online

ACCESS | Metrics & More | Article Recommendations | Supporting Information

ABSTRACT: Zero thermal expansion (ZTE) materials, keeping size constant as temperature varies, are valuable for resisting the deterioration of the performance from environmental temperature fluctuation, but they are rarely discovered due to the counterintuitive temperature−size effect. Herein, we demonstrate that a family of borates with sodalite cage structure, $Zn_4B_6O_{12}X$ (X = O, S, Se), exhibits intrinsic isotropic near-ZTE behaviors from 5 to 300 K. The very low thermal expansion is mainly owing to the coupling rotation of $[BO_4]$ rigid groups constrained by the bonds between Zn and cage-edged O atoms, while the central atoms in the cage have a negligible contribution. Our study has significant implications on the understanding of the ZTE mechanism and exploration of new ZTE materials.

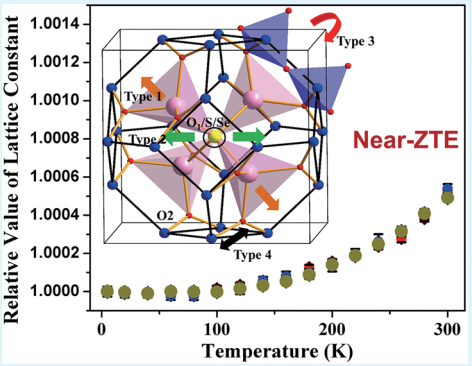

KEYWORDS: *intrinsic isotropic zero thermal expansion, phonon mode, first-principals vibration analysis, borate, sodalite cage structure*

INTRODUCTION

Zero thermal expansion (ZTE) materials, a type of functional materials that neither expand nor contract over a specific temperature range, can effectively eliminate the thermal stress, fatigue fracture, and microcracks to keep the performance stable when operated in high-temperature-fluctuating environments.[1] The ZTE effects are also tightly associated with a variety of basic physical properties in materials, covering element valence,[2] structural disorder,[3] magnetism,[4,5] ferroelectricity,[6,7] and phonon anharmonicity.[8] Thus, the explorations of ZTE materials have significant implications not only on the practical manufacturing and engineering but also on the understanding of basic physical mechanism. However, ZTE materials are rarely discovered owing to the counterintuitive temperature−size behavior, although they have been extensively studied for decades.

Up to now, the majority of ZTE materials were obtained by chemical doping or morphology manipulation on negative thermal expansion (NTE) materials[9,10] that inevitably introduces impurities and defects, and it would limit their practical applications. The achievement of intrinsic ZTE in perfect lattices is a very tough task since it is extremely difficult to obtain the subtle balance between the thermal expansion and contraction without external regulation. Moreover, for practical purposes, it is convenient to require the isotropic ZTE materials.[11−13] To our best knowledge, the intrinsic isotropic ZTE behavior has only been observed in a handful of materials, including $Fe[Co(CN)_6]$,[14] TaO_2F,[15] $MgZrF_6$,[11] and $K_6Cd_3(C_3N_3O_3)_4$.[16] Therefore, the research is highly desirable on the exploration of new intrinsic isotropic ZTE materials and the understanding of the underlying mechanisms.[17−21]

In the previous study, we proposed a "cage-restricting" model on the basis of phonon vibration mechanism, by which the intrinsic isotropic near-ZTE behavior was discovered in $Zn_4B_6O_{13}$(ZBO), a cubic borate with a sodalite-cage-like structure.[22] As depicted in Figure 1, each sodalite cage in ZBO is constructed by 24 $[BO_4]$ groups which are corner-shared by oxygens (O2) to form an enclosed $[B_{24}O_{48}]$ cage with the truncated octahedral shape. The $[B_{24}O_{48}]$ cage is fixed by four inside $[ZnO_4]$ tetrahedra that are connected to the same oxygen atom (O1) located at the center of the cage. We unraveled that the Zn−O2 bonds in $[ZnO_4]$ groups restrict the thermotropic rotation of rigid $[BO_4]$ groups and consequently thermal expansion of the sodalite cage. Thus, it results in the near-ZTE behavior in ZBO. However, the role of the Zn−O1 bonds in determining the temperature-induced size change of the sodalite cage remains unclear. The clarification of this issue would acquire a better understanding of the ZTE mechanism in the cage-restricting model. Moreover, following this structural model, more intrinsic ZTE materials are expected to be discovered.

Received: July 8, 2020
Accepted: August 6, 2020
Published: August 6, 2020

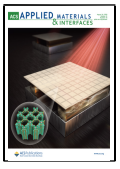

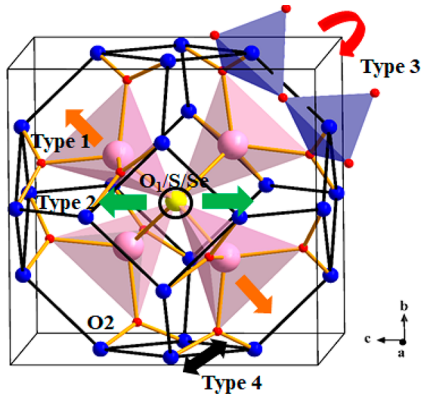

Figure 1. Crystal structure and schematic for the lattice vibration modes accounting for the thermal expansion in ZBO-type crystals. Zn, B, O1/S/Se, and O2 are represented by pink, blue, yellow, and red balls, respectively; the pink and cyan tetrahedra [ZnO_4] and [BO_4] are represented by pink and cyan tetrahedra, respectively. Type 1, 2, 3, and 4 lattice vibration modes are represented by orange, green, red, and dark arrows, respectively.

Inspired by this motivation, in this work, we replace the central oxygen atom O1 in the ZBO sodalite cage with the same VI-A group elements sulfur or selenium and obtain two isostructural compounds, $Zn_4B_6O_{12}S$ (ZBS) and $Zn_4B_6O_{12}Se$ (ZBSe). Interestingly, it is revealed that all the $Zn_4B_6O_{12}X$ (X= O, S, Se) compounds, independently of the center atoms in the cage, have almost the same isotropic near-ZTE coefficients. The origin of the near-ZTE behavior and the role of the different cage-central atoms in determining the thermal expansion of this type of materials is elaborated by lattice vibration analysis using the variable-temperature Raman spectra in combination with first-principles simulations.

EXPERIMENTAL AND COMPUTATIONAL METHODS

Synthesis. ZBO was synthesized by high-temperature solid phase reaction. ZnO (Sinopharm Chemical Reagent Co., Ltd., 99.7%) and B_2O_3 (Sinopharm Chemical Reagent Co., Ltd., 99.7%) were mixed in a ratio of 4:3 and fully grounded in air, slowly heated to 900 °C, and maintained at this temperature for 72 h. In order to avoid the volatilization of B_2O_3, we choose a slim (7 × Φ4 cm^3) cylindrical crucible equipped with a sealed lid. ZBS and ZBSe were synthesized with ZnO, ZnS/ZnSe (Macklin Biochemical Chemical Co., Ltd., 99.0%), and B_2O_3 mixed in a ratio of 3:1:3 and fully grounded under argon atmosphere in a glovebox. The ground mixture was placed in a quartz tube and packaged at a vacuum of 10^{-3} Pa and then slowly heated up to 900° and maintained at this temperature for 72 h. After cooling to room temperature, the target compound in powder form was obtained.

Variable-Temperature X-ray Diffraction (VTXRD) Measurements. The VTXRD measurements were performed in the temperature range from 5 to 300 K with a temperature interval of 20 K, using a Rigaku Smartlab 9 KW X-ray diffractometer with Cu Kα radiation (Kα1 = 1.5406 Å and Kα2 = 1.5443 Å). The scanning range is from 10° to 90° with 0.02 step size, and the scanning speed is 10°/min. The crystal structures at respective temperature were refined by the Rietveld method with TOPAS.[23,24] The PASCAL software was used to fit the thermal expansion coefficient.[25]

Variable-Temperature Raman Spectra (VTRS) Measurement. The VTRS measurements were performed in the temperature range from 93 to 293 K with an interval of 20 K, using a LabRAM HR Evolution Raman apparatus with the laser wavelength of 532 nm. The wavenumber scanning range is from 100 to 1300 cm^{-1}.

From the VTRS spectral data, the anharmonicity of lattice vibrations is characterized, by which the phonon modes accounting for thermal expansion can be assigned. The volume coefficients of thermal expansion (CTE) α_V, which is triple of linear CTE in an isotropic material, is defined by $\alpha_V = \frac{1}{B_0 V}\sum_i \gamma_i C_{Vi}(T)$,[26] where V is the molar volume, B_0 is the bulk modulus, C_{Vi} is the ith mode specific heat, and γ_i is the ith mode Grüneisen parameter. Since the former three variables are always positive, the contribution of the ith phonon mode to the CTE is determined by γ_i, which is defined by $\gamma_{iP} = \left(\frac{\delta \ln[\nu_i(P,T)]}{\delta \ln[V(P,T)]}\right)_P$,[27] where ν_i is the wavenumber of the ith Raman mode, and V is the molar volume. γ_{iP} can be obtained by the slopes of the $\ln(\nu_i)$−$\ln(V)$ curve deduced from the VTRS spectra.

First-Principles Calculations. The first-principles calculations were performed by the plane-wave pseudopotential method[28,29] implemented in the CASTEP package. The exchange-correlation term was described by the PBE[30] (Perdew, Burke, and Ernzerhof) functionals in the generalized gradient approximation (GGA).[31] The norm-conserving pseudopotentials were chosen to describe the ion−electron interactions.[32] The kinetic energy cutoff was set to 800.0 eV, and a 2 × 2 × 2 k-point composition Monkhorst−Pack grid was adopted.[33] Before the lattice vibration calculations, the crystal structures were optimized for cell parameters and atomic positions by the Broyden−Fletcher−Goldfarb−Shanno[34] (BFGS) method. To guarantee the computational accuracy, the convergence tolerance of energy, max force, max stress, and max displacement were set to 5.0 × 10^{-6} eV/atom, 0.01 eV/Å, 0.02 GPa, and 5.0 × 10^{-4} Å, respectively. The linear response method was used to calculated the atomic vibrational property,[35] in which the phonon frequencies were obtained by the second derivative of the total energy with respect to a given perturbation.

RESULTS AND DISCUSSION

The powder X-ray diffraction (XRD) spectra revealed that ZBO, ZBS, and ZBSe crystallize in the cubic space group $I\bar{4}3m$. The refined lattice constants of the three compounds at 300 K are 7.47607(16), 7.63863(12), and 7.68474(8) Å, respectively (Figure 2a). The increased lattice constants indicate that the

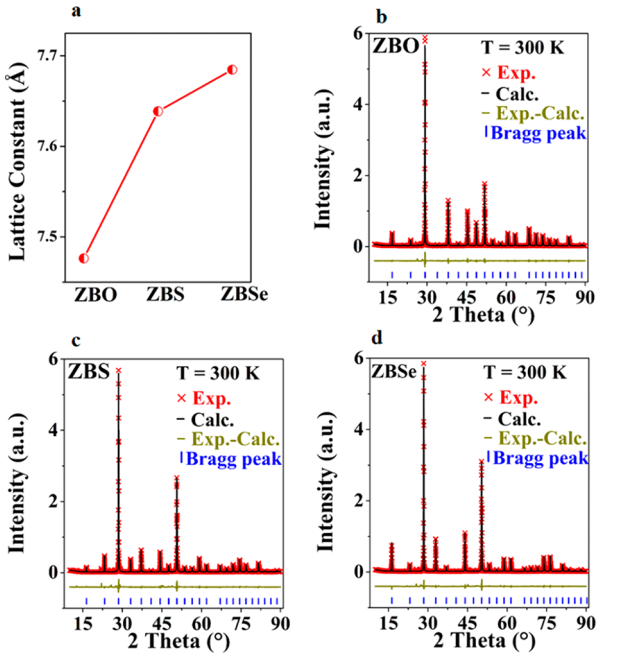

Figure 2. (a) Lattice constants of ZBO, ZBS, and ZBSe. The difference Rietveld plots of (b) ZBO, (c) ZBS, and (d) ZBSe for the XRD measurements at 300 K.

https://dx.doi.org/10.1021/acsami.0c12351
ACS Appl. Mater. Interfaces 2020, 12, 38435−38440

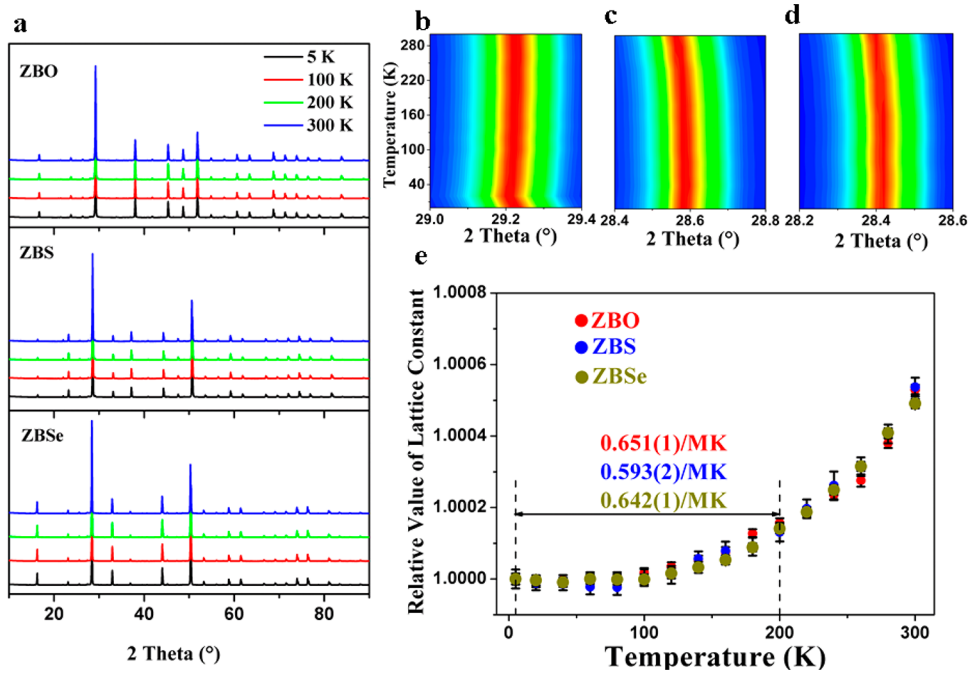

Figure 3. (a) VTXRD patterns of ZBO, ZBS, and ZBSe at various temperatures. (b), (c), and (d) Two-dimensional temperature contour map of the highest diffraction peak (corresponding to the (112) plane) in ZBO, ZBS, and ZBSe, respectively. (e) Variation of the cell parameters with respect to temperature in ZBO, ZBS, and ZBSe.

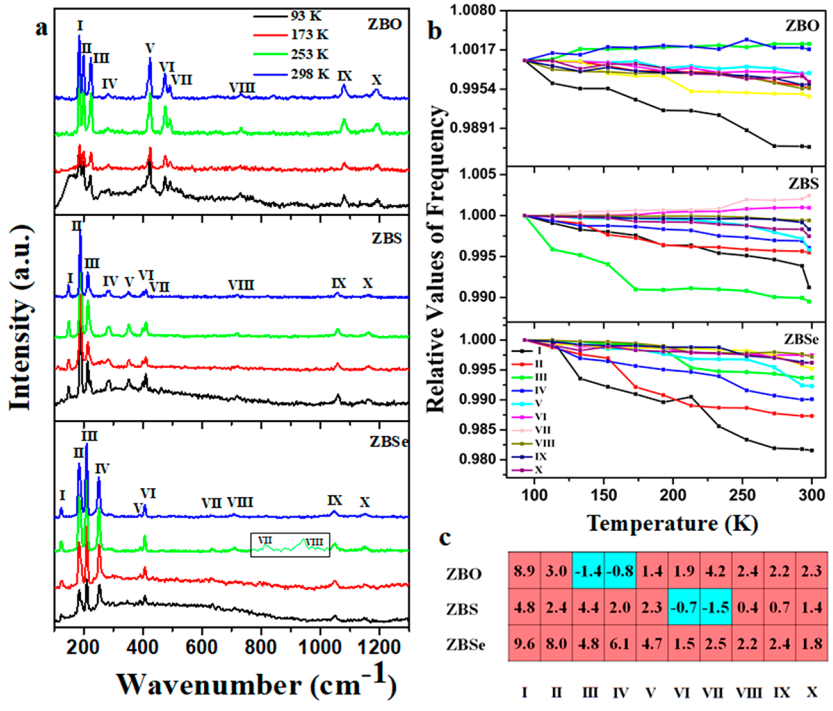

Figure 4. (a) VTRS spectra of ZBO, ZBS, and ZBSe. (b) Variation of the phonon modes with respect to increasing temperature in the Raman spectra of ZBO, ZBS, and ZBSe. (c) Isobaric Grüneisen parameters for the 10 principal Raman peaks in ZBO, ZBS, and ZBSe. The positive and negative values are represented by red and blue rectangles.

sulfur and selenium are substituted into the lattice sites. More importantly, using ZBO as the template with O1 replaced by sulfur and selenium, very good refinement results were obtained for the ZBS and ZBSe structures (Figure 2b–d), but the refinement fails when the O2 positions are assumed as replaced by sulfur and selenium, demonstrating that the S/Se atoms are substituted in the O1 sites only. Note that ZBS was synthesized for the first time in the present work, while the structure of ZBSe is consistent with that determined by Moran et al.[36]

The thermal expansion behaviors in ZBO, ZBS, and ZBSe from 5 to 300 K were investigated by VTXRD. As shown in Figure 3a, no new diffraction peak appears or old peak vanishes (also see Figure S1), indicating that no phase transition occurs

https://dx.doi.org/10.1021/acsami.0c12351
ACS Appl. Mater. Interfaces 2020, 12, 38435−38440

and all three compounds are thermodynamically stable in the measured temperature range. Moreover, for all three compounds, the positions of the highest diffraction peak ((112) plane) are almost unchanged as temperature increases (Figure 3b–d), suggesting weak thermal expansion. According to the refined cell parameters, the *a*-axes in ZBO, ZBS, and ZBSe increase by just 0.46% (from 7.47266 to 7.47607 Å), 0.51% (from 7.63470 to 7.63763 Å), and 0.51% (from 7.68084 to 7.68474 Å) from 5 to 300 K (Figure 3e and Table S1), corresponding to the fitted average linear CTE of 1.478(2)/MK. 1.540(5)/MK, and 1.554(2)/MK, respectively. These CTE values are much lower than those in the majority of materials, and thus the three compounds can be categorized as the near-ZTE materials, with the linear CTE comparable to other ever-reported ZTE materials, such as $MgZrF_6$[11] (−0.79/MK, 300–675 K), $Fe[Co(CN)_6]$[14] (−1.47/MK, 4.2–300 K), TaO_2F[15] (0.6/MK, 200–773 K), and $K_6Cd_3(C_3N_3O_3)_4$[16] (0.06/MK, 10–130 K). In particular, the cell parameters of ZBO, ZBS, and ZBSe are almost persistent between 5 and 200 K with the linear CTE of 0.651(1)/MK, 0.593(2)/MK, and 0.642(1)/MK, respectively, and the materials can be categorized into the ZTE class. Owing to their cubic structural symmetry, the near-ZTE behaviors in the three compounds are completely isotropic.

It is well-known that the thermal expansion is tightly associated with the thermotropic excitation of the lattice vibration phonon,[37−39] and thus the VTRS was employed to unravel the near-ZTE mechanism in ZBO, ZBS, and ZBSe.[40] As shown in Figure 4a, these compounds have 10 principal peaks in the Raman spectra, and the respective peaks are almost located at the same wavenumbers; they are defined as phonon mode I to mode X following the successive wavenumber order. As the temperature increases from 93 to 298 K, the phonon mode shifting for these compounds exhibits some different characteristics (Table S2 and Figure 4b): (i) for ZBO the modes III and IV are blue-shifted, while the other modes are red-shifted; (ii) for ZBS the modes VI and VII are blue-shifted, while the others are red-shifted; (iii) for ZBSe all modes are red-shifted. Because ZBO, ZBS, and ZBSe share almost the same CTE, the phonon modes dominantly determining the thermal expansion should exhibit the same evolution tendency with respect to the temperature. From the obtained Raman spectra, the isobaric mode Grüneisen parameters for the 10 principal mode peaks in three materials were calculated to determine the contribution of each mode to the CTE (Figure 4c and Table S2). It is revealed that the modes III and IV in ZBO, and modes VI and VII in ZBS, have negative mode Grüneisen parameters. In comparison, for ZBSe, there are no negative Grüneisen parameters existing for the 10 Raman modes. Because ZBO, ZBS, and ZBSe share almost the same CTE, the Grüneisen parameters contributing to the overall thermal expansion behaviors should exhibit the same evolution tendency with respect to temperature. Therefore, by comparing the phonon mode shifts and isobaric mode Grüneisen parameters, it is suggested that modes III, IV, VI, and VII have very little influence on the CTE of material, and the very low thermal expansion in the three compounds would be mainly determined by the red-shift of the modes I, II, V, VIII, IX, and X (Figure 4c).

To further shed light on the lattice vibration dominantly determining the weak thermal expansion, the first-principles phonon assignments were performed to project the phonon modes onto the respective atomic vibrations in real space. The calculated Raman spectra of ZBO, ZBS, and ZBSe are in good agreement with the experimental spectra at 298 K (Figure S3), confirming the feasibility of our first-principles phonon analysis. The detailed analysis reveals that the atomic vibrations can be categorized into four types (see Figure 1) according to the order of wavenumbers:[41−43] lateral vibration of the Zn atoms and Zn−O1/S/Se bonds (Type 1, Figure 1 and Figure S4a), transverse vibrations of the cage-center O1/S/Se atoms (Type 2, Figure 1 and Figure S4b), rotation of the $[BO_4]$tetrahedra (Type 3, Figure 1 and Figure S4c), and stretching of the B−O bonds (Type 4, Figure 1 and Figure S4d). Accordingly, we further assigned the contribution of the six thermal expansion-dependent phonon modes (I, II, V, VIII, IX, and X) to the atomic vibration types and then to thermal expansion: the phonon modes I and II are originated from the vibrations of zinc atoms (Type 1), which are not directly related to the size change of the sodalite cage. Because these modes are located at very low wavenumbers (<200 cm^{-1}), under low temperature only these modes could be excited, and thus the strictly ZTE behavior occurred between 5 and 100 K in the three compounds. On the other hand, the phonon modes IX and X are mainly related to the stretching of B−O bonds (Type 4). However, these modes are located at quite high wavenumbers (>1000 cm^{-1}), and they are hardly temperature-excited up to 300 K, since, at the same temperature, the excitation probability decreases as the phonon frequency increases, as also confirmed by the rather weak frequency-shifting of these modes on the variable-temperature Raman spectra (Figure 4b and Table S2). These phonon modes contribute little to the thermal expansion from 5 to 300 K. Thus, the thermal expansions of $Zn_4B_6O_{12}X$ are directly derived from the modes V and VIII, which are mainly the rotation modes among the rigid $[BO_4]$ tetrahedra in the sodalite $[B_{24}O_{48}]$ cage (Type 3). Note that, although the type 1 mode does not directly contribute to the thermal expansion, the Zn atoms are bonded with O2 atoms and their vibrations can cause the stretching of Zn−O2 bonds, which would further couple with and restrict the rotations of the $[BO_4]$ tetrahedra. We also analyzed the four thermal-expansion-independent modes (III, IV, VI, and VII) and found that these modes are mainly related to the transversal thermal vibrations of the cage-central O1/S/Se atoms (Type 2), which definitely do not affect the thermal expansion in this material family. Therefore, the near-ZTE properties in ZBO, ZBS, and ZBSe are due to the presence of thermal-expansion-insensitive $[B_{24}O_{48}]$ cages which are under the constraint of Zn−O2 bonds but are independent of the cage-central O1/S/Se atoms.

CONCLUSION

In this work, we demonstrated that the sodalite-cage-like borates, including ZBO, ZBS and ZBSe, possess almost the same intrinsic isotropic near-ZTE behavior from 5 to 300 K, which very scarcely occurs. Utilizing lattice vibration analysis based on variable-temperature Raman spectra combined with first-principles phonon assignment, it is demonstrated that the very low thermal expansion behavior of this type of structure is dominantly originated from the coupling rotation of $[BO_4]$ tetrahedra under the constraint of Zn−O2 bonds in $[B_{24}O_{48}]$ cages. The "cage-restricting" model with sodalite cage structure is irrespective of the cage-central atoms and thus provides an effective way to obtain the ZTE materials. This work established a complete structural model for the intrinsic ZTE behavior in perfect lattice, and, as believed, it has significant

https://dx.doi.org/10.1021/acsami.0c12351
ACS Appl. Mater. Interfaces 2020, 12, 38435−38440

implications on the understanding of the ZTE mechanism and the exploration of novel ZTE materials.

■ ASSOCIATED CONTENT

Supporting Information

The Supporting Information is available free of charge at https://pubs.acs.org/doi/10.1021/acsami.0c12351.

Cell parameters; the experimental and calculated Raman spectra; frequency of the vibrational modes in VTRS isobaric mode; Grüneisen parameters of ZBO/S/Se- (PDF)

Crystal structure and checkcif documents from 5 to 300 K of ZBO/S/Se (ZIP)

■ AUTHOR INFORMATION

Corresponding Authors

Xingxing Jiang − *Technical Institute of Physics and Chemistry, Chinese Academy of Sciences, Beijing 100190, China;* orcid.org/0000-0001-6068-8773; Email: xxjiang@mail.ipc.ac.cn

Zheshuai Lin − *Technical Institute of Physics and Chemistry, Chinese Academy of Sciences, Beijing 100190, China; University of Chinese Academy of Sciences, Beijing 100049, China;* orcid.org/0000-0002-9829-9893; Email: zslin@mail.ipc.ac.cn

Authors

Youquan Liu − *Technical Institute of Physics and Chemistry, Chinese Academy of Sciences, Beijing 100190, China; University of Chinese Academy of Sciences, Beijing 100049, China;* orcid.org/0000-0001-7979-1463

Dajiang Mei − *College of Chemistry and Chemical Engineering, Shanghai University of Engineering Science, Shanghai 201620, China*

Naizheng Wang − *Technical Institute of Physics and Chemistry, Chinese Academy of Sciences, Beijing 100190, China; University of Chinese Academy of Sciences, Beijing 100049, China;* orcid.org/0000-0002-2688-0400

Maxim S. Molokeev − *Laboratory of Crystal Physics, Kirensky Institute of Physics. Federal Research Center KSC SB RAS, Krasnoyarsk 660036, Russia; Department of Physics, Far Eastern State Transport University, Khabarovsk 680021, Russia; Siberian Federal University, Krasnoyarsk 660041, Russia*

Complete contact information is available at: https://pubs.acs.org/10.1021/acsami.0c12351

Author Contributions

¶These authors contributed equally.

Notes

The authors declare no competing financial interest.

■ ACKNOWLEDGMENTS

This work was supported by the National Scientific Foundations of China (Grants 51872297, 51702330, 11974360, 51972208, 51890864, and 51802321), Russian Foundation for Basic Research (Grant 17-52-53031), and Fujian Institute of Innovation (FJCXY18010201) in CAS. X.J. acknowledges the support from the Youth Innovation Promotion Association in CAS (Grant 2017035) and Youth Talent Promotion Project from China Association for Science and Technology.

■ ABBREVIATIONS

ZTE, zero thermal expansion; NTE, negative thermal expansion; CTE, coefficient of thermal expansion; ZBO, $Zn_4B_6O_{13}$; ZBS, $Zn_4B_6O_{12}S$; ZBSe, $Zn_4B_6O_{12}Se$; VTXRD, variable-temperature X-ray diffraction; VTRS, variable-temperature Raman spectra; PBE, Perdew, Burke, and Ernzerhof; GGA, generalized gradient approximation; BFGS, Broyden−Fletcher−Goldfarb−Shanno

■ REFERENCES

(1) Chen, J.; Hu, L.; Deng, J.; Xing, X. Negative Thermal Expansion in Functional Materials: Controllable Thermal Expansion by Chemical Modifications. *Chem. Soc. Rev.* **2015**, *44* (11), 3522−3567.

(2) Salvador, J. R.; Guo, F.; Hogan, T.; Kanatzidis, M. G. Zero Thermal Expansion in YbGaGe due to an Electronic Valence Transition. *Nature* **2003**, *425* (6959), 702−705.

(3) Morelock, C. R.; Greve, B. K.; Cetinkol, M.; Chapman, K. W.; Chupas, P. J.; Wilkinson, A. P. Role of Anion Site Disorder in the Near Zero Thermal Expansion of Tantalum Oxyfluoride. *Chem. Mater.* **2013**, *25* (9), 1900−1904.

(4) Song, X. Y.; Sun, Z. H.; Huang, Q. Z.; Rettenmayr, M.; Liu, X. M.; Seyring, M.; Li, G. N.; Rao, G. H.; Yin, F. X. Adjustable Zero Thermal Expansion in Antiperovskite Manganese Nitride. *Adv. Mater.* **2011**, *23* (40), 4690−4694.

(5) Song, Y.; Qiao, Y.; Huang, Q.; Wang, C.; Liu, X.; Li, Q.; Chen, J.; Xing, X. Opposite Thermal Expansion in Isostructural Noncollinear Antiferromagnetic Compounds of Mn_3A (A = Ge and Sn). *Chem. Mater.* **2018**, *30* (18), 6236−6241.

(6) Chen, J.; Fan, L.; Ren, Y.; Pan, Z.; Deng, J.; Yu, R.; Xing, X. Unusual Transformation from Strong Negative to Positive Thermal Expansion in $PbTiO_3$-$BiFeO_3$ Perovskite. *Phys. Rev. Lett.* **2013**, *110* (11), 115901.

(7) Ren, Z.; Zhao, R.; Chen, X.; Li, M.; Li, X.; Tian, H.; Zhang, Z.; Han, G. Mesopores Induced Zero Thermal Expansion in Single-Crystal Ferroelectrics. *Nat. Commun.* **2018**, *9* (1), 1638.

(8) Ticknor, J. O.; Hester, B. R.; Adkins, J. W.; Xu, W.; Yakovenko, A. A.; Wilkinson, A. P. Zero Thermal Expansion and Abrupt Amorphization on Compression in Anion Excess ReO_3-Type Cubic $YbZrF_7$. *Chem. Mater.* **2018**, *30* (9), 3071−3077.

(9) Zhu, H.; Li, Q.; Yang, C.; Zhang, Q. H.; Ren, Y.; Gao, Q. L.; Wang, N.; Lin, K.; Deng, J. X.; Chen, J.; Gu, L.; Hong, J. W.; Xing, X. R. Twin Crystal Induced near Zero Thermal Expansion in SnO_2 Nanowires. *J. Am. Chem. Soc.* **2018**, *140* (24), 7403−7406.

(10) Song, Y.; Chen, J.; Liu, X.; Wang, C.; Zhang, J.; Liu, H.; Zhu, H.; Hu, L.; Lin, K.; Zhang, S.; Xing, X. Zero Thermal Expansion in Magnetic and Metallic $Tb(Co,Fe)_2$ Intermetallic Compounds. *J. Am. Chem. Soc.* **2018**, *140* (2), 602−605.

(11) Xu, J. L.; Hu, L.; Song, Y. Z.; Han, F.; Qiao, Y. Q.; Deng, J. X.; Chen, J.; Xing, X. R. Zero Thermal Expansion in Cubic $MgZrF_6$. *J. Am. Ceram. Soc.* **2017**, *100* (12), 5385−5388.

(12) Sleight, A. W. Isotropic Negative Thermal Expansion. *Annu. Rev. Mater. Sci.* **1998**, *28*, 29−43.

(13) Takenaka, K.; Takagi, H. Zero Thermal Expansion in a Pure-Form Antiperovskite Manganese Nitride. *Appl. Phys. Lett.* **2009**, *94* (13), 131904.

(14) Margadonna, S.; Prassides, K.; Fitch, A. N. Zero Thermal Expansion in a Prussian Blue Analogue. *J. Am. Chem. Soc.* **2004**, *126* (47), 15390−15391.

(15) Tao, J. Z.; Sleight, A. W. Very Low Thermal Expansion in TaO_2F. *J. Solid State Chem.* **2003**, *173* (1), 45−48.

(16) Xia, M. J.; Liang, F.; Meng, X. H.; Wang, Y. G.; Lin, Z. S. Intrinsic Zero Thermal Expansion in Cube Cyanurate $K_6Cd_3(C_3N_3O_3)_4$. *Inorg. Chem. Front.* **2019**, *6* (9), 2291−2295.

(17) Tallentire, S. E.; Child, F.; Fall, I.; Vella-Zarb, L.; Evans, I. R.; Tucker, M. G.; Keen, D. A.; Wilson, C.; Evans, J. S. O. Systematic and Controllable Negative, Zero, and Positive Thermal Expansion in Cubic $Zr_{1-x}Sn_xMo_2O_8$. *J. Am. Chem. Soc.* **2013**, *135* (34), 12849−12856.

(18) Lind, C. Two Decades of Negative Thermal Expansion Research: Where Do We Stand? *Materials* **2012**, *5* (6), 1125−1154.
(19) Goodwin, A. L.; Calleja, M.; Conterio, M. J.; Dove, M. T.; Evans, J. S. O.; Keen, D. A.; Peters, L.; Tucker, M. G. Colossal Positive and Negative Thermal Expansion in the Framework Material Ag_3 $Co(CN)_6$. *Science* **2008**, *319* (5864), 794−797.
(20) Liu, Z.; Gao, Q.; Chen, J.; Deng, J.; Lin, K.; Xing, X. Negative Thermal Expansion in Molecular Materials. *Chem. Commun.* **2018**, *54* (41), 5164−5176.
(21) Yamada, I.; Marukawa, S.; Hayashi, N.; Matsushita, M.; Irifune, T. Room-temperature Zero Thermal Expansion in a Cubic Perovskite Oxide $SrCu_3Fe_{4-x}Mn_xO_{12}$. *Appl. Phys. Lett.* **2015**, *106* (15), 151901.
(22) Jiang, X. X.; Molokeev, M. S.; Gong, P. F.; Yang, Y.; Wang, W.; Wang, S. H.; Wu, S. F.; Wang, Y. X.; Huang, R. J.; Li, L. F.; Wu, Y. C.; Xing, X. R.; Lin, Z. S. Near-Zero Thermal Expansion and High Ultraviolet Transparency in a Borate Crystal of $Zn_4B_6O_{13}$. *Adv. Mater.* **2016**, *28* (36), 7936−7940.
(23) Bruker AXS TOPAS V4, General Profile and Structure Analysis Software for Powder Diffraction Data. *User's Manual*; Bruker AXS: Karlsruhe, Germany, 2008.
(24) Rietveld, H. M. A Profile Refinement Method for Nuclear and Magnetic Structures. *J. Appl. Crystallogr.* **1969**, *2*, 65−71.
(25) Cliffe, M. J. G. A. L.; Goodwin, A. L. Pascal: a Principal Axis Strain Calculator for Thermal Expansion and Compressibility Determination. *J. Appl. Crystallogr.* **2012**, *45*, 1321−1329.
(26) Liu, Y. M.; Wang, Z. H.; Wu, M. Y.; Sun, Q.; Chao, M. J.; Jia, Y. Negative Thermal Expansion in Isostructural Cubic ReO_3 and ScF_3: a Comparative Study. *Comput. Mater. Sci.* **2015**, *107*, 157−162.
(27) Zhou, L.; Mernagh, T. P.; Mo, B.; Wang, L.; Zhang, S.; Wang, C. Raman Study of Barite and Celestine at Various Temperatures. *Minerals* **2020**, *10* (3), 260.
(28) Clark, S. J.; Segall, M. D.; Pickard, C. J.; Hasnip, P. J.; Probert, M. J.; Refson, K.; Payne, M. C. First Principles Methods Using CASTEP. *Z. Kristallogr. - Cryst. Mater.* **2005**, *220* (5−6), 567−570.
(29) Payne, M. C.; Teter, M. P.; Allan, D. C.; Arias, T. A.; Joannopoulos, J. D. CASTEP 4.2 Academic Version, Licensed under the UKCP-MSI Agreement Rev. *Rev. Mod. Phys.* **1992**, *64*, 1045.
(30) Perdew, J. P.; Burke, K.; Ernzerhof, M. Generalized Gradient Approximation Made Simple. *Phys. Rev. Lett.* **1996**, *77* (18), 3865−3868.
(31) Perdew, J. P.; Wang, Y. Pair-Distribution Function and its Coupling-Constant Average for the Spin-Polarized Electron-Gas. *Phys. Rev. B: Condens. Matter Mater. Phys.* **1992**, *46* (20), 12947−12954.
(32) Hamann, D. R.; Schluter, M.; Chiang, C. Norm-Conserving Pseudopotentials. *Phys. Rev. Lett.* **1979**, *43* (20), 1494−1497.
(33) Monkhorst, H. J.; Pack, J. D. Special Points for Brillouin-Zone Integrations. *Phys. Rev. B* **1976**, *13* (12), 5188−5192.
(34) Pfrommer, B. G.; Cote, M.; Louie, S. G.; Cohen, M. L. Relaxation of Crystals with the Quasi-Newton Method. *J. Comput. Phys.* **1997**, *131* (1), 233−240.
(35) Baroni, S.; de Gironcoli, S.; Dal Corso, A.; Giannozzi, P. Phonons and Related Crystal Properties from Density-Functional Perturbation Theory. *Rev. Mod. Phys.* **2001**, *73* (2), 515−562.
(36) Moran, K. L.; Gier, T. E.; Harrison, W. T. A.; Stucky, G. D.; Eckert, H.; Eichele, K.; Wasylishen, R. E. Synthesis and Characterization of Mixed ZnSe/GaP Semiconductor Species Included in the Sodalite Structure. *J. Am. Chem. Soc.* **1993**, *115* (23), 10553−10558.
(37) Bridges, F.; Keiber, T.; Juhas, P.; Billinge, S. J. L.; Sutton, L.; Wilde, J.; Kowach, G. R. Local Vibrations and Negative Thermal Expansion in ZrW_2O_8. *Phys. Rev. Lett.* **2014**, *112* (4), 045505.
(38) Ernst, G.; Broholm, C.; Kowach, G. R.; Ramirez, A. P. Phonon Density of States and Negative Thermal Expansion in ZrW_2O_8. *Nature* **1998**, *396* (6707), 147−149.
(39) Hancock, J. N.; Turpen, C.; Schlesinger, Z.; Kowach, G. R.; Ramirez, A. P. Unusual Low-Energy Phonon Dynamics in the Negative Thermal Expansion Compound ZrW_2O_8. *Phys. Rev. Lett.* **2004**, *93* (22), 225501.
(40) Cheng, X.; Yuan, J.; Zhu, X.; Yang, K.; Liu, M.; Qi, Z. Origin of Negative Thermal Expansion in Zn_2GeO_4 Revealed by High Pressure Study. *J. Phys. D: Appl. Phys.* **2018**, *51* (9), 095303.
(41) Gava, V.; Martinotto, A. L.; Perottoni, C. A. First-Principles Mode Gruneisen Parameters and Negative Thermal Expansion in α-ZrW_2O_8. *Phys. Rev. Lett.* **2012**, *109*, 195503.
(42) Wang, F.; Xie, Y.; Chen, J.; Fu, H.; Xing, X. R. First-Principles Study on Negative Thermal Expansion of $PbTiO_3$. *Appl. Phys. Lett.* **2013**, *103* (22), 221901.
(43) Curti, M.; Mendive, C. B.; Bredow, T.; Murshed, M. M.; Gesing, T. M. Structural, Vibrational and Electronic Properties of $SnMBO_4$ (M = Al, Ga): a Predictive Hybrid DFT Study. *J. Phys.: Condens. Matter* **2019**, *31* (34), 345701.

https://dx.doi.org/10.1021/acsami.0c12351
ACS Appl. Mater. Interfaces 2020, 12, 38435−38440